Effect of Hammer Length and Nonlinear Paperribbon Characteristics on Impact Printing

Abstract: An analysis of the impact process in a particular type of high-speed printer was undertaken to determine the effect of hammer length on the contact time. The hammer is modeled as a one dimensional wave propagation medium and the paper-ribbon combination as a dissipative, nonlinear medium with hysteresis. The integrated macroscopic viscoelastic parameters for a particular impact geometry and hammer momentum were determined from a combination of the analytical model and the experiments run on an instrumented printer robot. Permanent deformation of the paper-ribbon caused by character penetration was also determined in this manner. The simulated model was then used to predict the change in dynamic behavior of such a system due to variations of the hammer length. The hammer length is shown to have only a tertiary effect on contact time in such a dissipative deformable nonlinear system. This result demonstrates that the widely discussed use of hammer length as a design parameter to control contact time in impact printing is invalid for such a dissipative system.

Introduction

Impact printing, in the mechanism studied in this work, is a complex mechanical process involving a hammer, a paper-ribbon combination and a typeslug. As in most high speed printers, the dynamics of this print mechanism are a major determinant of the ultimate speed attainable. In particular, the duration of contact between the paperribbon combination and the hammer is an important design factor, affecting both mechanical speed and the print transfer process. Of the dynamic parameters controlling contact time, hammer momentum is one obvious concern but is strongly constrained by the energy and force requirements of print transfer. Less obvious are the effects of elastic wave propagation in the hammer and the effects of the nonlinear, dissipative, deformable medium represented by the paper and ribbon. Discussions in recent times, based to a large extent on classical elastic wave propagation arguments, have indicated that hammer length is especially significant. It is shown, however, that the dissipative behavior of the paper-ribbon medium has considerably more effect than hammer length in a printer of the type considered here.

To evaluate the relative importance of the various dynamic properties, data were taken from a series of experimental measurements made on an instrumented printer robot, which was essentially an IBM 1403-II with the chain at rest (for easier instrumentation). The analytical

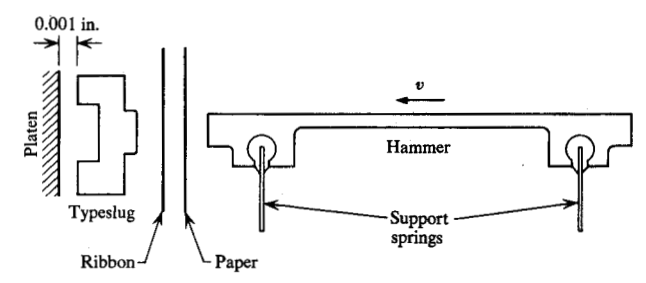


Figure 1 IBM 1403-II printer hammer mechanism.

model was derived by considering the functional mechanisms that would be possible during impact and combining their effects mathematically.

1403-II printing mechanism

The mechanism under study is shown in Fig. 1. The hammer is actuated by the armature of a magnet with an initial velocity of 100 in./sec. The hammer and the typeslug each have a mass of 2.2 g. The print action takes place as the paper-ribbon combination is squeezed between the hammer and the typeslug. The stationary platen, a laminate of steel and elastomer, is spaced about 0.001 in. from the typeslug. Each typeslug mounts two characters and is fastened to a steel tape that moves in a

direction perpendicular to the hammer motion. In the robot the tape is at rest.

• Experimental method

The robot was constructed in order to determine what happens during printing. Strain gages were used to monitor the forces near the end of the hammer and in the legs of the typeslug. Also, optical reflection techniques were used to continuously measure the displacement of the hammer. This measurement was used to determine the velocity before and after impact.

To test the effect of the hammer length on the printing process, six different hammers were constructed. Three hammers were straight rods with lengths of one, two and three inches. The other three hammers were modeled after IBM 1403-II printer hammers and had the same set of lengths. Each hammer had a mass of 2.2 g.

A typical record of force in the hammer and in the typeslug legs is shown in Fig. 2. This experiment was performed with the two-inch IBM 1403 printer hammer but is typical of all the hammer configurations. In all cases, the force-time curve for the hammer had the double peak shown and the maximum force in the typeslug legs occurred between the two hammer peaks. Also, note that there is no force in the typeslug legs until about the time of the first maximum in the hammer force curve.

Analytical model of the print mechanism

In this section, we describe the mathematical model for simulating the force-time curves of the experiments. The hammer is considered to be a long, thin rod capable of transmitting longitudinal stress waves. The paper and ribbon are taken to be a highly nonlinear, dissipative medium. The typeslug is allowed to translate and rotate but is constrained in this motion by the pressure of the platen.

Hammer model

An IBM 1403-II printer hammer (shown in Fig. 1) is assumed to be an elastic body capable of transmitting one-dimensional stress waves. While this is not strictly true because of the complicated geometry, the assumption will allow us to show that contact time does not depend on wave propagation. A more exact theory would not alter this conclusion since the time scale of mechanical events will be shown to be long as compared with wave propagation times.

A portion of a hypothetical hammer is shown in Fig. 3. The hammer is taken to be composed of several prismatic segments. If the thickness of each segment is small compared to the wavelengths involved, a one-dimensional analysis is valid.

The assumption of one-dimensional wave propagation leads to the following equations, which govern the motion.

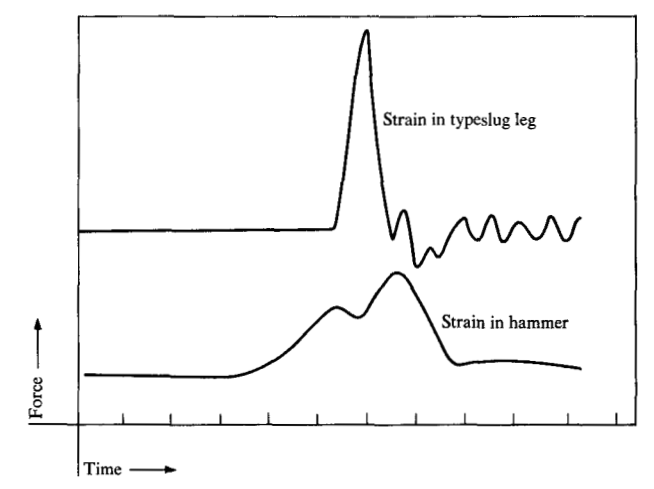
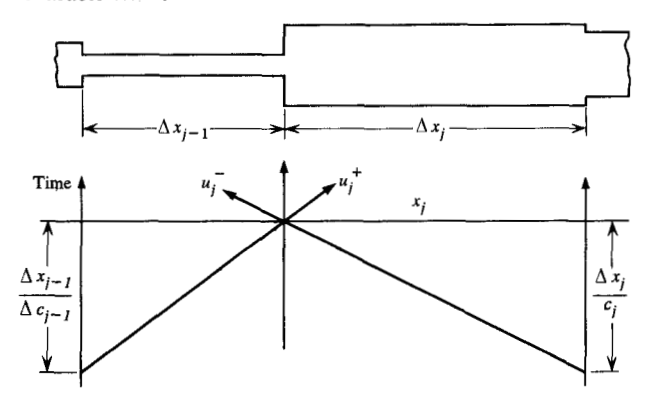


Figure 2 Strain records in hammer and typeslug. Upper trace: strain in legs of typeslug. Lower trace: strain near impacting end of the hammer. (20 μsec/division.)

Figure 3 Segment of hypothetical hammer and its wave characteristics,



$$F_i = A_i' E_i \frac{\partial u_i}{\partial x_i}; \qquad (1)$$

$$\frac{\partial F_i}{\partial x_i} = \rho_i A_i \frac{\partial^2 u_i}{\partial t^2}.$$
 (2)

Equation (1) is a statement of Hooke's law in one dimension where A_i ' is the virtual area of the *j*th cross section, E_i Young's modulus, F_i the total force in the section, and u_i the displacement at the point x_i and time t. A virtual area, instead of the actual area, is used to take into account the fact that a very short segment of the hammer will not have uniform stress over a cross section if the segments on either side are much smaller in cross section. Equation (2) results from Newton's second law of motion. The quantity A_i is the area of the section and ρ_i is the density of the material.

If Eqs. (1) and (2) are combined, we obtain the wave equation for the jth segment:

$$\frac{\partial^2 u_i}{\partial x_i^2} - \frac{1}{c_i^2} \frac{\partial^2 u_i}{\partial t^2} = 0, \text{ where } c_i^2 = E_i A_i' / \rho_i A_i.$$
 (3)

This equation must be solved subject to the interface conditions, the latter being that force F_i and velocity v_i are continuous across segment interfaces. These conditions are expressed as

$$v_i^+(0, t) = v_i^-(0, t);$$
 (4)

$$A_{i-1}{}'E_{i-1} \frac{\partial u_i^-(0,t)}{\partial x_i} = A_i{}'E_i \frac{\partial u_i^+(0,t)}{\partial x_i},$$
 (5)

where the + and - indicate values taken just beyond and just in front of the interface, respectively.

We express the solution to the wave equation as a D'Alembert solution; i.e., in terms of forward and backward traveling waves,

$$v_{i}^{+}(x_{i}, t) = v_{i+}(t - x_{i}/c_{i}) + y_{i+}(t + x_{i}/c_{i}) + V_{0}, \quad x_{i} > 0; \quad (6)$$

$$v_{i}(x_{i}, t) = v_{i-}(t + x_{i}/c_{i}) + y_{i-}(t - x_{i}/c_{i-1}) + V_{0}, \quad x_{i} < 0, \quad (7)$$

where V_0 is the initial velocity.

The displacement u_i can be expressed as

$$u_i^-(x_i, t) = u_{i-1}(t + x_i/c_{i-1}) + w_{i-1}(t - x_i/c_{i-1}) + V_0t,$$
 (8)

where u_i and w_i are the displacement amplitudes of backward and forward traveling waves respectively. The strain is

$$\frac{\partial u_i^-(x_i, t)}{\partial x_i} = \frac{1}{c_{i-1}} \left[u_{i-1}'(t + x_i/c_{i-1}) + w_{i-1}'(t - x_i/c_{i-1}) \right], \tag{9}$$

where the prime denotes differentiation with respect to the argument. Similarly, the velocity can be written as

$$v_{i}^{-} = \frac{\partial u_{i}^{-}(x_{i}, t)}{\partial t} = u_{i-}'(t + x_{i}/c_{i-1}) + w_{i-}'(t - x_{i}/c_{i-1}) + V_{0}.$$
(10)

Therefore, we can use the fact that $v_{i-} = u_{i-}'$ and $y_{i-} = w_{i-}'$ to obtain our desired expression,

$$\frac{\partial u_i^-(x_i, t)}{\partial x_i} = c_{i-1}^{-1} [v_{i-}(t + x_i/c_{i-1}) - y_{i-}(t - x_i/c_{i-1})].$$
(11)

Of course, there is an expression similar to Eq. (11) for $\partial u_i^+/\partial x_i$.

We now have expressions for all the quantities that occur in the interface conditions. The substitution of these expressions into the interface conditions yields the following relations:

$$v_{i+}(t) + y_{i+}(t) = v_{i-}(t) + y_{i-}(t);$$
 (12)

$$(A_{i-1}'E_{i-1}/c_{i-1})[v_{i-1}(t) - y_{i-1}(t)]$$

$$= (A_i'E_i/c_i)[-v_{i+}(t) + y_{i+}(t)].$$
 (13)

We now observe that

$$y_{i-}(t) = v_{i-1,+}(t - \Delta x_{i-1}/c_{i-1});$$
 (14)

$$y_{i+}(t) = v_{i+1,-}(t - \Delta x_i/c_i).$$
 (15)

These conditions are valid because the equations give the values of a velocity at two different points on the same characteristic. Equations (12) and (13) can be solved for $v_{i\pm}$ in terms of $v_{i\pm1\pm}$ at an earlier time by using Eqs. (14) and (15). This solution is

$$v_{i-}(t) = (z_{i-1} + z_i)^{-1} [2z_i v_{i+1,-}(t - \Delta x_i/c_i) + (z_{i-1} - z_i) v_{i-1,+}(t - \Delta x_{i-1}/c_{i-1})];$$
(16)

$$v_{j+}(t) = (z_{j-1} + z_j)^{-1} [2z_{j-1}v_{j-1,+}(t - \Delta x_{j-1}/c_{j-1}) + (z_j - z_{j-1})v_{j+1,-}(t - \Delta x_j/c_j)].$$
(17)

The quantities z_i are impedances given by

$$z_{i} = (A_{i}A_{i}'E_{i}\rho_{i})^{\frac{1}{2}}.$$
 (18)

At the left-hand boundary (where the impact occurs) the force is given by

$$F_{\rm b} = A_1 E_1 \left. \frac{\partial u_1}{\partial x_1} \right|_{x_1 = 0} \tag{19}$$

The boundary values are

$$\frac{\partial u_1}{\partial x_1}\Big|_{x_1=0} = c_1^{-1} [-v_{1+}(t) + v_{2-}(t - \Delta x_1/c_1)] \text{ and } (20)$$

$$\left. \frac{\partial u_1}{\partial t} \right|_{z_1 = 0} = v_{1+}(t) + v_{2-}(t - \Delta x_1/c_1) + V_0. \tag{21}$$

Therefore, combining Eqs. (19), (20) and (21), we can write

$$\left. \frac{\partial u_1}{\partial t} \right|_{z_1=0} = V_0 - (c_1 F_b / A_1 E_1) + 2 v_{2-} (t - \Delta x_1 / c_1).$$
(22)

The boundary condition at the right-hand end of the hammer can be satisfied by setting the impedance in the Nth section (there are N-1 actual sections) to zero. Therefore, the boundary condition becomes

$$v_{N-}(t) = v_{N-1,+}(t - \Delta x_{N-1}/c_{N-1}). \tag{23}$$

• Typeslug model

The typeslug, shown in Fig. 4, is assumed to be a rigid mass with translational and rotational degrees of freedom. The rotation is about an axis perpendicular to the cross section shown. Before the hammer strikes the paperribbon combination, the typeslug is about 0.001 in. from the platen. The force of impact drives the typeslug into the platen. There is assumed to be a spring restoring force between the legs of the typeslug and the platen. Also, in series with this spring is a dashpot that simulates the effect of energy carried away in the form of stress waves. The equations of motion for the slug are

$$\frac{dU_{\rm m}}{dt} = V_{\rm m}; \tag{24}$$

$$\frac{dV_{\rm m}}{dt} = (F_{\rm b} - F_{\rm a} - F_{\rm c})/M_{\rm m}; \tag{25}$$

$$\frac{d\theta}{dt} = W;$$
 and (26)

$$\frac{dW}{dt} = [a_{\rm a}(F_{\rm e} - F_{\rm a}) - F_{\rm b}a_{\rm b} - k_{\rm t}\theta]/M_{\rm m}k^2, \qquad (27)$$

where $U_{\rm m}$ and $V_{\rm m}$ are the displacement and velocity, respectively, of the center of mass, $M_{\rm m}$ is the mass of the slug and k is the radius of gyration. The constant $k_{\rm t}$ is the spring constant for a torsional spring. This spring represents the rotational restraint of the steel tape and neighboring typeslugs that tend to keep the typeslug from rotating. The displacement of the platen, $U_{\rm p}$, is governed by the equation

$$C_{\rm p} \frac{dU_{\rm p}}{dt} = F_{\rm p} = F_{\rm a} + F_{\rm c} \tag{28}$$

where the forces F_a and F_c in the legs of the typeslug are functions of the displacements x_a and x_c . That is,

$$F_{\mathbf{a}} = k_1(x_{\mathbf{a}}); \tag{29}$$

$$F_{\rm c} = k_1(x_{\rm c}), \tag{30}$$

where

$$x_{\rm a} = U_{\rm m} + \theta a_{\rm a} - U_{\rm p} \quad \text{and} \tag{31}$$

$$x_{\rm e} = U_{\rm m} - \theta a_{\rm a} - U_{\rm p}. \tag{32}$$

The function k_1 represents a nonlinear spring that has zero force when the slug is not in contact with the platen and behaves as a linear spring when they are in contact. This can be expressed as

$$k_1(x) = (x + U_{m0})k_{11},$$
 $x < -U_{m0}$
= 0, $x \ge -U_{m0}$, (33)

where U_{m0} is the initial gap between the legs of the typeslug and the platen and k_{11} is the linear spring constant.

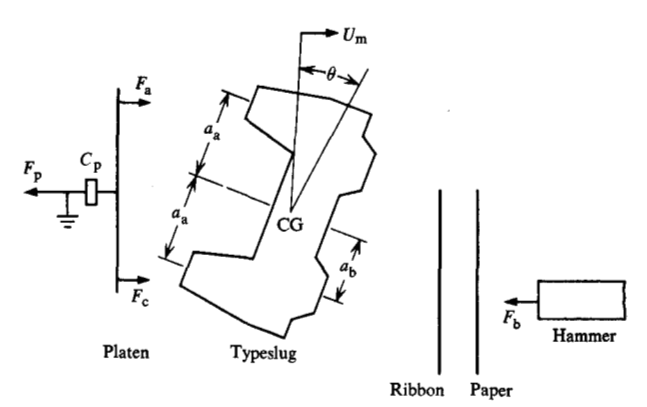


Figure 4 Typeslug, ribbon, paper and platen combination.

• Paper-ribbon combination

A model of the impact phenomena in this dissipative, nonlinear deformable medium must describe the functional behavior of the events that can be expected to take place. The printing impact clearly transfers ink, embosses the paper and transfers elastic energy to other areas. A number of physical events obviously take place: Air is squeezed out from between paper and ribbon and from among paper fibers; ink is squeezed through fibers and surfaces; air is compressed, fibers are compressed and ink is compressed; and fibers are permanently deformed. Many of these events are similar in nature and can be described by the same functional representation; there are viscous losses due to air and ink flow; nonlinear elastic effects due to the compressible nature of air, ink and paper fibers; and permanent deformation of paper and ribbon fibers. Our model combines these similar effects together and deals only with the lumped parameters for such similar mechanisms. The model proposed here consists of three major parts to describe the paper-ribbon combination in impact: a nonlinear spring, viscous losses and permanent deformation. In the discussion that follows, a heuristic explanation is given for each of these aspects of the model. However, as noted, the model details should not be taken too literally. For example, although the nonlinear spring characteristic is developed from the compression of air between the paper-ribbon combination and the platen, several other mechanisms could have produced similar nonlinear force-deflection curves. The effect of each one is included in the lumped parameter for this type of behavior. The same point can be made for the viscous losses and permanent deformation aspects of this model. The important point is that the behavior of the model supports and explains the physically observable results.

The paper-ribbon combination is taken to be two large, flat parallel plates. Air is trapped between them but can leak out at the ends. The configuration is shown

$$\frac{1}{P}\frac{dP}{dt} = -\frac{1}{V}\left[\frac{dV}{dt} + Q\right]. \tag{34}$$

The volume V is related to the displacement by

$$V = A(x_0 + x), \tag{35}$$

where A is the area of the plates and x_0 is the initial air gap. The force F on the plates is related to the pressure P by

$$F = -A(P - P_0), \tag{36}$$

where P_0 is the atmospheric pressure. If Eqs. (35) and (36) are substituted into Eq. (34), the following relation is obtained

$$dF/dt = (P_0A - F)(dx/dt + Q/A)/(x_0 + x).$$
 (37)

In the special case for which there is no leakage (Q = 0), this equation can be integrated to yield

$$F = P_0 A x / (x_0 + x). (38)$$

If we let $k_2 = P_0 A/x_0$, then the relation can be written as

$$F = k_2 x / (1 + x / x_0). ag{39}$$

The quantity k_2 has the dimensions of a spring constant and, in fact, is the spring constant in the limit of small displacement. As the paper is compressed, the value of x becomes more negative and the "spring" becomes stiffer. This compaction process fits a heuristic argument that attributes a stiffening of the equivalent spring to an increase in density of the system. Thus we have a model for a two-parameter nonlinear spring, and the parameters have physical meaning. The spring constant k_2 is determined from the slope of the force-deflection curve at the origin and x_0 is the maximum deformation that the paper-ribbon combination can withstand.

It is necessary to have a relationship among the leakage Q, the force and the displacement. This relationship states that the leakage is proportional to the force F and proportional to the square of the gap between the ribbon and paper. These assumptions yield the relation

$$Q = F(1 + x/x_0)^2/C_2, (40)$$

where C_2 is a damping constant.

The assumption that the leakage is proportional to the square of the paper-ribbon separation is made on heuristic grounds. It indicates that as the ribbon and paper come closer together it is harder for the air to leak out. The leakage is therefore obviously related to the gap between the ribbon and paper and decreases with decreasing gap. That is, there are viscous losses that depend on velocity and these losses diminish as the point of maximum compression is reached. As noted, other

Table 1 Parameters used in numerical experiments.

Parameter	Value	Units	
. ρ	0.000736 (steel)	lb sec²/in.4	
ρ	0.000259 (alumin	num) lb sec ² /in. ⁴	
\boldsymbol{E}	30×10^6 (steel)	lb/in.2	
\boldsymbol{E}	10×10^6 (alumin	num) lb/in.2	
V_0	100	in./sec	
$M_{ m m}$	1.182×10^{-5}	lb sec2/in.	
	or 2.1	grams	
$U_{ m m0}$	0.00065	in.	
$a_{\rm a}$	0.09	in.	
a_{b}	0.06	in.	
\boldsymbol{k}	0.09	in.	
$k_{ m t}$	2500	lb in.	
Print	Area of	Virtual area	Incremental
hammer	section (in.2)	of section (in.2)	length (in.)
————— 1 in.	A = 0.01645	A' = 0.00987	$\Delta x = 1.0$
2 in.	$A_1 = 0.01476$	$A_1' = 0.009$	$\Delta x_1 = 0.372$
	$A_2 = 0.0041$	$A_2' = 0.0041$	$\Delta x_2 = 1.222$
	$A_3 = 0.01476$	$A_3' = 0.009$	$\Delta x_3 = 0.406$
3 in.			
(aluminum	A = 0.0157	A' = 0.0157	$\Delta x = 3.0$

microflow losses will have similar dependencies and their effects have been lumped together in the various parameters of the model.

One other loss factor is introduced that allows for the crushing of the paper and ribbon fibers. We let the spring constant k_2 take on different values depending on whether the paper-ribbon medium is being compressed or whether it is expanding. As the paper and ribbon are compressed, they act as a relatively soft spring. During this compression, however, fibers are being permanently deformed and broken and there is permanent macroscopic deformation. As the hammer and typeslug begin to separate, the compressed paper-ribbon combination acts as a harder spring. This effect is introduced in the model by using two spring constants k_{21} and k_{22} . The constant k_{21} is used during compression and k_{22} is used during expansion. Therefore we set

$$k_2 = k_{21},$$
 $dx/dt < 0;$
 $k_2 = k_{22},$ $dx/dt \ge 0;$ (41)

where $k_{22} \geq k_{21}$.

Numerical experiments

The model as used in the numerical experiments is defined by Eqs. (16), (17), (23-30), (33) and (42); the parameters of the model are defined in Table 1. The initial conditions are that $v_{i\pm}(t) = 0$ when $t \le 0$. New velocities are com-

puted at each time step from Eqs. (16) and (17). Linear interpolation is used to find values of $v_{i\pm}(t)$ at earlier times when the characteristic does not coincide with a point for which the velocity has been computed. The set of ordinary differential equations that describes the model was solved numerically by using a fourth-order Runge-Kutta scheme [1] and the IBM APL\360 terminal system. The use of a terminal system greatly facilitated program debugging. More importantly, the interactive nature of the terminal system allows one to experiment numerically to determine realistic values for the parameters involved.

Results

Most of the parameters in the model could be determined from simple measurements or known values. These include the elastic modulus of the hammer, the mass of the typeslug and the initial velocity of the hammer. A few of the parameters were determined from the experiments run on the printer robot. For example, the effective spring constant of the typeslug-platen combination was measured by determining the length of time the slug is in contact with the platen and using the relation

$$T = \pi \sqrt{M_{\rm m}/k_{11}}. \tag{42}$$

It is well known that if a thin prismatic bar traveling in the axial direction strikes a rigid wall, the contact time is twice the length of time it takes for a wave to travel one length of the bar; that is, contact time t_C is

$$t_{\rm C} = 2L/c, \tag{43}$$

where L is the length of the bar and c is the wave speed. In order to test the model of the hammer, several numerical experiments were performed in which the hammer struck a fairly stiff spring. These results are shown in Fig. 5. Note that for the three-inch hammer, the contact time is approximately 2L/c (30 μ sec).

The shape of the two-inch hammer is not well approximated by a prism. Because the mass is concentrated at the ends, we obtain a force-time curve as shown in Fig. 5(b). When the bar is not a prism, there is not a simple relationship to predict the contact time because of the many wave reflections at the discontinuities. However, it is clear that without losses the dynamics and thus the contact time are indeed determined by the elastic wave propagation in the hammer system if the impacted medium is stiff compared with the elasticity of the hammer.

If, instead of striking a stiff spring, the hammer impacts on paper and a ribbon that are backed by a stiff spring, we obtain the force-time curves shown in Fig. 6. Notice now that there is not a great deal of difference in the impact force-time relationships and contact times among hammers of zero, one, two and three inches. Thus, in contrast with the above cases, the behavior of the soft

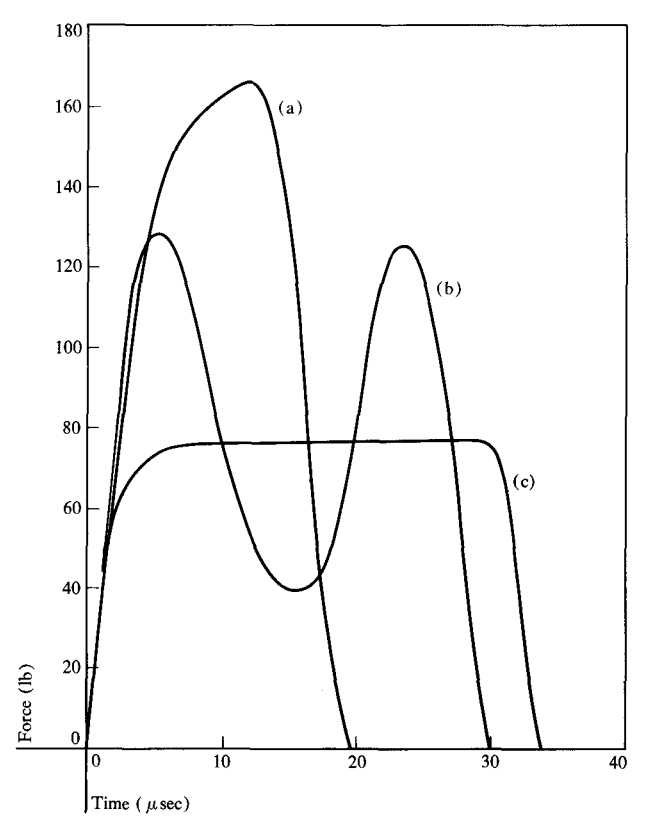
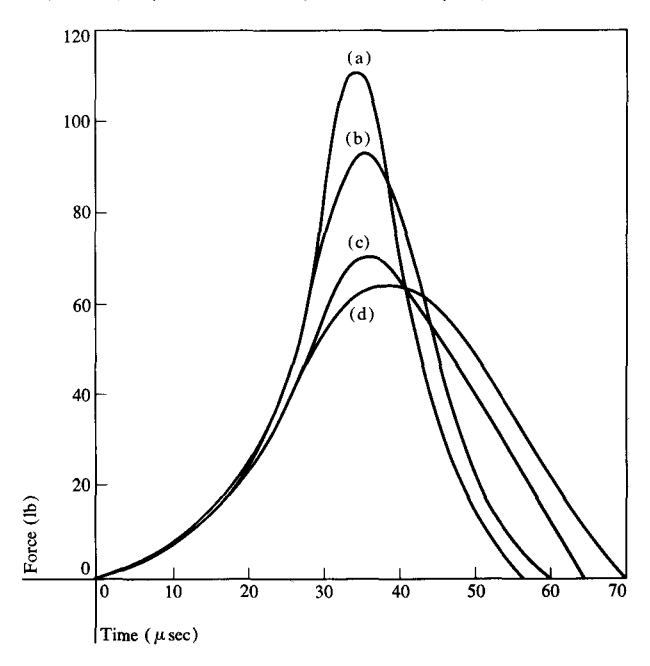


Figure 5 Force-time curves for (a) one-inch, (b) two-inch and (c) three-inch hammer striking stiff spring. $(k = 5 \times 10^5 \text{ lb/in.})$.

Figure 6 Force-time curve for (a) lumped mass, (b) one-inch hammer, (c) two-inch hammer and (d) three-inch hammer striking ribbon-paper combination ($k_{zz} = 5000 \text{ lb/in.}$, $k_{zz} = 10,000 \text{ lb/in.}$, $x_0 = 0.003 \text{ in.}$, $c_2 = 1 \text{ lb sec/in.}$).



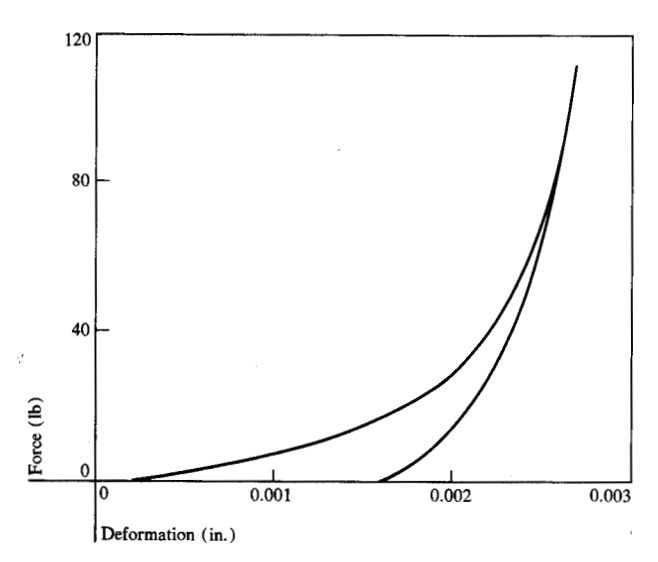
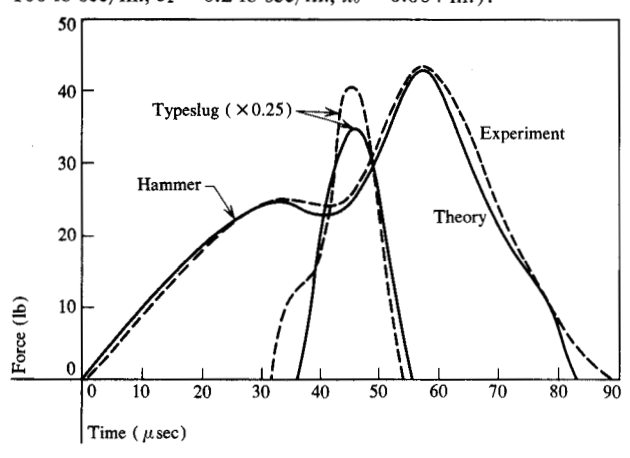


Figure 7 Hysteresis curve. Same conditions as Fig. 6.

Figure 8 Force-time curves for hammer and typeslug (k = 250,000 lb/in., $k_{21} = 10,000 \text{ lb/in.}$, $k_{22} = 20,000 \text{ lb/in.}$, $c_1 = 100 \text{ lb sec/in.}$, $c_2 = 0.2 \text{ lb sec/in.}$, $x_0 = 0.004 \text{ in.}$).



paper-ribbon combination dominates the dynamic solution. The parameters of the paper model were obtained by running the computer model several times and adjusting the parameters until responses close to the experimental results were obtained. It should be pointed out that this is currently the only way to obtain values for these parameters and is the technique used in all the work reported here. These parameters, because of their macroscopic nature, depend on the geometry of the contact area, and on the force and velocity curves of the system. This impact geometry dependence is easily envisioned if one considers the case of a dot or a period being the impact form rather than the flat hammer face. The same initial and dynamic conditions before impact would result in

markedly different viscous losses. The greater stresses under the dot would cause much higher embossing or permanent deformation and fiber destruction and the air flow and microflow losses would be of different order. At the present time, no microscopic or point model of the impact process exists with parameters independent of these factors. Thus, any independent determination of, say, the damping parameter would depend on the conditions under which the experiment was run. In order to ascertain the value of this parameter for the ranges of force and displacement covered in the simulation, the same experimental conditions and impact geometry must be used. A hysteresis curve for the case of a lumped mass striking the ribbon and paper is shown in Fig. 7. These data were computed from the same run as shown in Fig. 6(a). The force is plotted as a function of displacement in the ribbon-paper combination and the area inside the curve is equal to the energy extracted from the hammer.

The simulation with all the elements in the model, i.e., the platen, typeslug, ribbon, paper and hammer, indicates that in this case it does not matter significantly whether the hammer is considered as a lumped mass or a threeinch bar. The effect of the paper and ribbon, along with the movable typeslug, completely dominates the wave propagation in the hammer. The force-time curve computed using our model is compared with the experimental results in Fig. 8. It is interesting to note that the parameters that describe the behavior of the paper-ribbon combination in this case are not the same as when the typeslug is absent. This is due, as indicated, to the fact that with the character present the stresses are much higher. The force is distributed over the area of the type character instead of over the entire face of the hammer. In fact, the force-time curve depends on the particular character being struck. These experiments were all performed by striking the "8". Other experiments performed by striking a "period" occasioned much lower forces because there was more penetration by the character. This observation underlines the fact that the dissipative characteristics of the impact process are extremely sensitive to the detailed geometries of the impacting surfaces. It has been noted that there is a marked difference in impact losses even when gross geometries are kept the same but surface conditions are changed, e.g., the impact in air on a paperribbon-platen combination by a rod, first with a polished end and then with a scored end. To make engineering comparisons of the factors such as we have done, care must be taken to keep the interface characteristics and impact dynamics the same. Therefore, the momentum of the hammer was kept constant throughout all tests. This allowed us to duplicate the impact loss factors and make meaningful comparisons of the dynamic differences due to changes in hammer length. Figure 8 is the forcetime curve computed for the two-inch hammer. The

114

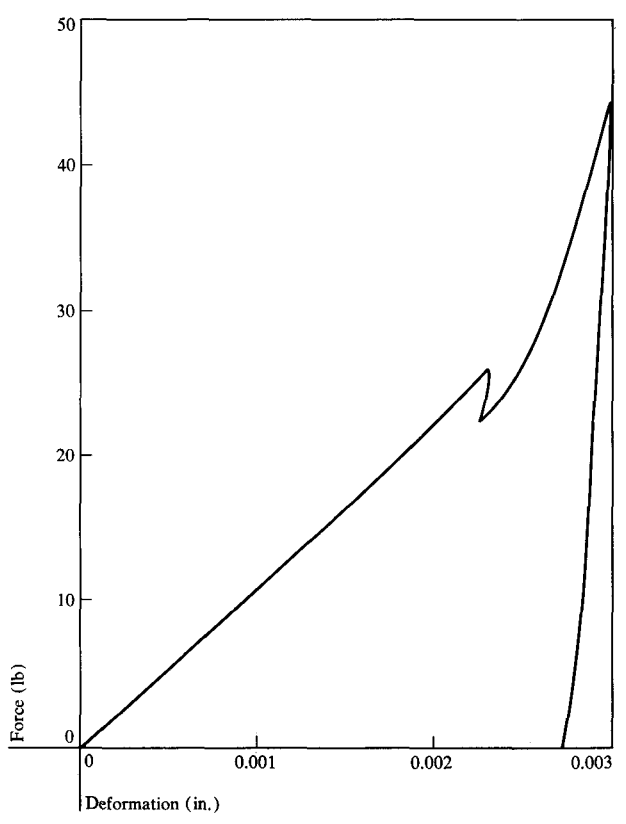


Figure 9 Hysteresis curve. Same run as Fig. 8.

results for a point-mass hammer, a one-inch and a three-inch hammer essentially coincide with this curve. Again it is shown that the behavior of the typeslug and the paper-ribbon combination have much more influence on the dynamic aspects of printing than does the length of the hammer.

Figure 9 shows the hysteresis curve for the case shown in Fig. 8. Much more energy is absorbed by the paper-ribbon combination in this case than in the case of the hammer only. This is due to the presence of the type character, which causes more permanent deformation and different microflow losses.

The double peak in the force-time curve in Fig. 8 and the spike-like reversal in the hysteresis curve are due to the inertia of the typeslug as it is accelerated from rest and before it hits the platen. After striking the platen, the typeslug rebounds at about the same speed as that at which it hits. It then imparts this momentum to the hammer, causing the hammer to rebound and producing the second peak in the force-time curve.

Experimental runs on multicopy printing indicated, as expected, that the prolongation of the contact time further masked any hammer effects. A generally less dissipative system was observed due almost certainly to the reduction in embossing or permanent deformation.

Conclusions

A model for the impact print mechanism of a high-speed printer has been developed that describes all of the salient features of the process. This model has been used to determine the effect of hammer length on contact time. It is found that the dynamic behavior of the ribbon and paper can be modeled as a lumped system characterized by a nonlinear spring, a nonlinear dashpot, and hysteresis. This nonlinear, dissipative behavior completely masks the effect of hammer length. Therefore, in analyzing the printing process, it is far more important to accurately model the behavior of the ribbon and paper than it is to include the effect of wave propagation in the hammer.

Acknowledgments

The authors express their appreciation to C. B. Smith who directed the experimental work, and to S. Tsao for his assistance with the numerical methods.

Reference

 M. J. Romanelli, "Runge-Kutta methods for the solution of ordinary differential equations," *Mathematical Meth*ods for Digital Computers, John Wiley and Sons, Inc., New York 1960.

Received July 2, 1970

The authors are located at the IBM Systems Development Division Laboratory, Endicott, New York 13760.